

Five-dimensional collective Hamiltonian with improved inertial functions

Kouhei Washiyama,^{1,2,*} Nobuo Hinohara,^{1,3} and Takashi Nakatsukasa^{1,3,4}

¹Center for Computational Sciences, University of Tsukuba, Tsukuba 305-8577, Japan

²Research Center for Superheavy Elements, Kyushu University, Fukuoka 819-0395, Japan

³Faculty of Pure and Applied Sciences, University of Tsukuba, Tsukuba 305-8571, Japan

⁴RIKEN Nishina Center, Wako 351-0198, Japan

(Dated: March 4, 2024)

Background: To describe shape fluctuations associated with large-amplitude collective motion in the quadrupole degrees of freedom, the five-dimensional collective Hamiltonian (5DCH) has been widely used. The inertial functions in the 5DCH are microscopically calculated with the energy density functional (EDF) theory employing the cranking formula. However, since the cranking formula ignores dynamical residual effects, it is known to fail to reproduce the correct inertial functions, for instance, the total mass for the translational motion.

Purpose: We aim to resolve problems of the insufficient description of the inertial functions in the 5DCH. We provide a practical method to include the dynamical residual effects in the inertial functions that depend on the quadrupole deformation parameters β and γ .

Methods: We use the local quasiparticle random-phase approximation (LQRPA) based on the constrained Hartree-Fock-Bogoliubov states in the β - γ plane with the Skyrme EDF. The finite-amplitude method is used for efficient computations of the LQRPA.

Results: The inertial functions evaluated with the LQRPA significantly increase from the ones with the cranking formula due to the dynamical residual effects. This increase also shows a strong β - γ dependence. We show an application of the present method to a transitional nucleus ^{110}Pd . The low-lying positive-parity spectra are well reproduced with the LQRPA inertial functions.

Conclusions: We clarify the importance of the dynamical residual effects in the inertial functions of the 5DCH for the description of the low-lying spectra. The 5DCH with the improved inertial functions provides a reliable and efficient description of low-lying spectra in nuclei associated with the quadrupole shape fluctuation.

Introduction. A proper and feasible description of the shape dynamics in the ground and the excited states is one of the important subjects in nuclear physics. Observations of spectroscopic properties in nuclei suggest the existence of shape fluctuations and shape coexistence phenomena in low-lying states in nuclei, particularly in the so-called transitional regions from spherical to deformed shapes in the nuclear chart [1].

The self-consistent nuclear energy density functional (EDF) theory has often been employed to describe ground-state properties of nuclei [2, 3]. To describe shape fluctuations and shape coexistence phenomena associated with large-amplitude collective motion, it is necessary to use beyond-mean-field methods. The generator-coordinate method (GCM) with the quadrupole deformation parameters β and γ as generator coordinates [4–9] has been developed and shown the importance of including the triaxial degree of freedom, γ . Recently, the standard GCM was extended to construct the basis states stochastically [10, 11] and variationally [12]. Although the GCM is a fully quantum theory, in practice, we need to combine the GCM with the projection method to recover the broken symmetries. The GCM with the projection method requires a large amount of numerical computations. In addition, there remain many unsolved issues with realistic EDFs [3]. For instance, the discontinuities

and divergences are caused by the fractional powers of the density dependence in EDFs [13, 14].

As an alternative approach to the GCM, the five-dimensional collective Hamiltonian (5DCH) method [15, 16] with the intrinsic quadrupole deformation parameters (β, γ) and the three Euler angles has been extensively used based on the EDF [16–20]. In most of the EDF-based 5DCH studies, the inertial functions in the vibrational and rotational kinetic energies are calculated according to the formula in the adiabatic perturbation [21], which is identical to the well-known Inglis-Belyaev (IB) formula for the rotational moment of inertia [22, 23]. The vibrational masses are further approximated by the so-called perturbative cranking formula [24]. The cranking formula ignores variation of the self-consistent potential induced by the collective motion, known as the dynamical residual effects, thus, giving an insufficient description of the inertial functions [25]. In particular, the absence of the time-odd terms of the dynamical mean field leads to the violation of the Galilean symmetry and is known to produce the wrong translational mass [26]. Despite such drawbacks, the cranking formula has been widely used [16–20], because the full inclusion of the dynamical residual effects in the inertial functions requires a huge computational cost. Some recent 5DCH studies [20, 27] evaluate the rotational moments of inertia within the cranked Hartree-Fock-Bogoliubov (HFB) framework that are equivalent to the Thouless-Valatin inertia [28] to include the dynamical residual effects in the rotational kinetic energy. In many of the former studies, a phe-

* E-mail: washiyama@nucl.ph.tsukuba.ac.jp

nomenological enhancement factor of 1.2–1.4 is adopted for the inertial functions evaluated with the cranking formula.

To properly include the dynamical residual effects in the inertial functions, the constrained HFB (CHFb) plus local quasiparticle random-phase approximation (LQRPA) was proposed in Ref. [29]. Practical applications of the CHFb + LQRPA in the β - γ plane were performed only with the semi-realistic pairing-plus-quadrupole (P + Q) Hamiltonian [29–33]. Note that, for axially symmetric shapes without the γ degree of freedom, there have been a few attempts with the Skyrme EDF [34, 35]. These studies showed the importance of the dynamical residual effects in the inertial functions.

Our goal is to construct the 5DCH for the Skyrme EDF with the inertial functions including the dynamical residual effects. To overcome the numerical difficulties, we employ the finite-amplitude method (FAM) [36] that gives the response to an external one-body field. The result of the FAM is equivalent to that of the QRPA linear-response calculation, while the computational cost of the FAM is significantly lower than that of the QRPA. The FAM has been applied to various objectives [37–52]. The formulation with the FAM for the inertia associated with zero-energy modes was given in Ref. [46], and applied to the inertia for pairing rotations [46, 47] and that for spatial rotations [53, 54]. The present study is an extension of the methods developed in Refs. [35, 46] to the inertial functions in the 5DCH with β and γ .

5DCH method. The five-dimensional quadrupole collective Hamiltonian is given as [15]

$$H_{\text{coll}} = T_{\text{vib}} + T_{\text{rot}} + V(\beta, \gamma), \quad (1)$$

$$T_{\text{vib}} = \frac{1}{2} D_{\beta\beta}(\beta, \gamma) \dot{\beta}^2 + D_{\beta\gamma}(\beta, \gamma) \dot{\beta} \dot{\gamma} + \frac{1}{2} D_{\gamma\gamma}(\beta, \gamma) \dot{\gamma}^2, \quad (2)$$

$$T_{\text{rot}} = \frac{1}{2} \sum_{k=1}^3 \mathcal{J}_k(\beta, \gamma) (\omega_k^{\text{rot}})^2, \quad (3)$$

where the collective potential V and all the inertial functions appearing in the vibrational T_{vib} and rotational T_{rot} kinetic energies depend on β and γ . The inertial functions $D_{\beta\beta}$, $D_{\beta\gamma}$, $D_{\gamma\gamma}$, and $\mathcal{J}_k(\beta, \gamma) = 4\beta^2 D_k(\beta, \gamma) \sin^2(\gamma - 2\pi k/3)$ denote the vibrational masses and the rotational moments of inertia, respectively. ω_k^{rot} are the rotational angular velocities in the body-fixed frame. We use the Pauli prescription to quantize the Hamiltonian (1) and obtain the excitation energies and collective wave functions. More details of the 5DCH method can be found in Refs. [16, 29, 55].

The collective potential is given by the energy at the state $|\phi(\beta, \gamma)\rangle$ obtained by solving the CHFb equation with constraints on the mass quadrupole operators $\hat{Q}_{20} = \sum_{i=1}^A r_i^2 Y_{20}(\hat{r}_i)$ and $\hat{Q}_{22} = \sum_{i=1}^A r_i^2 [Y_{22}(\hat{r}_i) + Y_{2-2}(\hat{r}_i)]/\sqrt{2}$. The quadrupole deformation parameters are written as $\beta \cos \gamma = \eta Q_{20} = \eta \langle \phi(\beta, \gamma) | \hat{Q}_{20} | \phi(\beta, \gamma) \rangle$ and $\beta \sin \gamma = \eta Q_{22} = \eta \langle \phi(\beta, \gamma) | \hat{Q}_{22} | \phi(\beta, \gamma) \rangle$ with $\eta =$

$4\pi/(3R^2 A)$ and $R = 1.2A^{1/3}$ fm of the mass number A .

Inertial functions. The CHFb+LQRPA inertial functions in the β - γ plane are given in Ref. [29]. Although the LQRPA are defined at each CHFb state $|\phi(\beta, \gamma)\rangle$, for simplicity, we abbreviate $|\phi(\beta, \gamma)\rangle$ as $|\phi\rangle$ in the following.

We employ the FAM [36] for a solution of the LQRPA equation for the Skyrme EDF, which provides the X and Y amplitudes induced by an external field \hat{F} at a given frequency ω . Following Refs. [35, 46], the relation between the amplitudes (X, Y) and the local generators (\hat{Q}_i, \hat{P}_i) for the i th normal mode with the eigenfrequency Ω_i is given in their two-quasiparticle (2qp) components as

$$X_{\mu\nu}(\omega; \hat{F}) = \sum_i \frac{1}{\omega^2 - \Omega_i^2} (P_{\mu\nu}^i + i\omega Q_{\mu\nu}^i) p_i(\hat{F}), \quad (4a)$$

$$Y_{\mu\nu}(\omega; \hat{F}) = \sum_i \frac{1}{\omega^2 - \Omega_i^2} (-P_{\mu\nu}^{i*} - i\omega Q_{\mu\nu}^{i*}) p_i(\hat{F}), \quad (4b)$$

where we fix the normalization of (\hat{Q}_i, \hat{P}_i) to make the local inertial mass $M_i = 1$ [35]. Here, \hat{F} , \hat{Q}_i , and \hat{P}_i are all Hermitian. Their 2qp components $F_{\mu\nu}$ and $Q_{\mu\nu}^i$ are chosen to be real, while $P_{\mu\nu}^i$ are pure imaginary. In Eq. (4), the pure imaginary quantities $p_i(\hat{F})$ are given by

$$p_i(\hat{F}) \equiv \langle \phi | [\hat{P}_i, \hat{F}] | \phi \rangle = \sum_{\mu < \nu} (P_{\mu\nu}^{i*} - P_{\mu\nu}^i) F_{\mu\nu}. \quad (5)$$

The FAM response function, $S_{\hat{F}', \hat{F}}(\omega)$, for Hermitian and real operators, \hat{F} and \hat{F}' , is defined as

$$S_{\hat{F}', \hat{F}}(\omega) \equiv \sum_{\mu < \nu} \left[F_{\mu\nu}'^{20*} X_{\mu\nu}(\omega; \hat{F}) + F_{\mu\nu}^{02*} Y_{\mu\nu}(\omega; \hat{F}) \right] \quad (6)$$

$$= \sum_i \frac{1}{\omega^2 - \Omega_i^2} p_i(\hat{F}) p_i^*(\hat{F}'). \quad (7)$$

Then, a contour integration of Eq. (7) with a contour C_i that encloses the pole $\omega = \Omega_i$ in the complex energy plane,

$$\frac{1}{2\pi i} \oint_{C_i} \omega S_{\hat{F}', \hat{F}}(\omega) d\omega = \frac{1}{2} p_i(\hat{F}) p_i^*(\hat{F}') \quad (8)$$

gives $p_i(\hat{Q}_{20})$ and $p_i(\hat{Q}_{22})$ by proper choices of the operators F and F' .

We select two LQRPA normal modes for the collective coordinates q_i ($i = 1, 2$). The prescription for this selection is given in Ref. [29] (see also *Numerical procedure* below). The kinetic energy of the LQRPA normal modes in the diagonal form is rewritten in terms of the collective variables Q_{2m} ($m = 0, 2$) as

$$T_{\text{vib}} = \frac{1}{2} \sum_{i=1,2} \dot{q}_i^2 = \frac{1}{2} \sum_{m,n=0,2} \mathcal{M}_{mn} \dot{Q}_{2m} \dot{Q}_{2n}, \quad (9)$$

where the vibrational inertia tensor \mathcal{M}_{mn} is obtained by

$$\mathcal{M}_{mn} = \sum_{i=1,2} \frac{\partial q_i}{\partial Q_{2m}} \frac{\partial q_i}{\partial Q_{2n}}. \quad (10)$$

The inverses of these partial derivatives are evaluated as

$$\begin{aligned} \frac{\partial Q_{2m}}{\partial q_i} &= \frac{\partial}{\partial q_i} \langle \phi | \hat{Q}_{2m} | \phi \rangle \\ &= \langle \phi | [\hat{Q}_{2m}, \frac{1}{i} \hat{P}_i] | \phi \rangle = ip_i(\hat{Q}_{2m}). \end{aligned} \quad (11)$$

Thus, the inertia tensor (10) is obtained by the FAM calculation of $p_i(\hat{Q}_{2m})$ in Eq. (7) through Eq. (11).

With the relation between (β, γ) and (Q_{20}, Q_{22}) , the vibrational masses $D_{\beta\beta}$, $D_{\beta\gamma}$, and $D_{\gamma\gamma}$ are obtained from \mathcal{M}_{00} , \mathcal{M}_{02} , and \mathcal{M}_{22} in Eq. (10) [29]. Note that the formulation given above can be extended to cases with more than two collective variables.

For the rotational moments of inertia, the Thouless-Valatin rotational moment of inertia \mathcal{J}_k at the CHFB state $|\phi\rangle$ is evaluated from the FAM strength function at zero energy as $S_{\hat{J}_k, \hat{J}_k}(\omega = 0) = -\mathcal{J}_k$, where \hat{J}_k is the angular momentum operator [46].

Numerical procedure. We solve the CHFB + LQRPA equations following Ref. [35]. We calculate the vibrational masses with the FAM-LQRPA in two steps. First, to find peaks in the strength distribution, we solve the FAM equations with the external fields \hat{Q}_{20} and \hat{Q}_{22} at $0 \leq |\omega| \leq 4$ MeV, in both real and imaginary ω with a smearing width of 0.01 MeV. The peak position should correspond to the LQRPA poles Ω_i . Second, for each pole, we perform the contour integration (8) with a circle of radius 0.02 MeV discretized to eight points. Then, we select the two most collective LQRPA modes following the prescription [29] that a pair of LQRPA solutions that give the minimum value of $W = (D_{\beta\beta}D_{\gamma\gamma} - D_{\beta\gamma}^2)/\beta^2$ is selected from many LQRPA solutions. In practice, we select several peaks with large strengths and calculate Eq. (8) with all the combinations from the selected peaks to find the minimum W .

We solve the CHFB equations with the two-basis method [56, 57] in the three-dimensional Cartesian mesh with a $(13.2 \text{ fm})^3$ box with a mesh size of 0.8 fm. The reflection symmetries about $x = 0$, $y = 0$, and $z = 0$ planes lead to the single-particle states as eigenstates of the parity, z signature, and y -time simplex [58–61]. The single-particle basis consists of 1400 neutron and 1120 proton HF-basis states, which approximately correspond to the maximum quasiparticle energy of 60 MeV for ^{110}Pd and give a good convergence in the CHFB and LQRPA calculations [35]. We employ the SkM* EDF [62] and the contact volume-type pairing with a pairing window of 20 MeV above and below the Fermi level as described in Ref. [60]. The pairing strengths are adjusted to reproduce the empirical neutron and proton gaps in ^{106}Pd . We use an equilateral triangular mesh of $\Delta\beta \approx 0.05$ in $0 < \beta < 0.6$ and $0^\circ < \gamma < 60^\circ$ in the β - γ plane, consisting of 93 deformation points.

The numerical calculations of the FAM are performed with hybrid parallelization (MPI + OpenMP). For the vibrational masses, it takes about 480 core hours to select several peaks in the strength distributions and

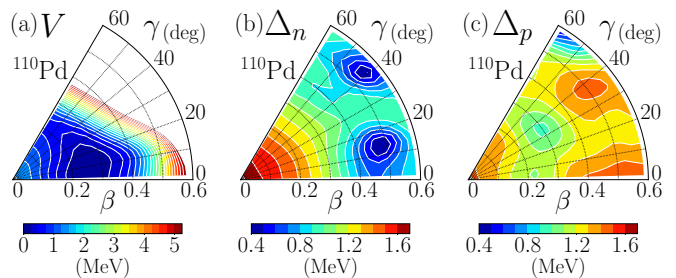


FIG. 1. Potential energy surface (a) and pairing gaps for neutrons (b) and protons (c) in the β - γ plane in ^{110}Pd .

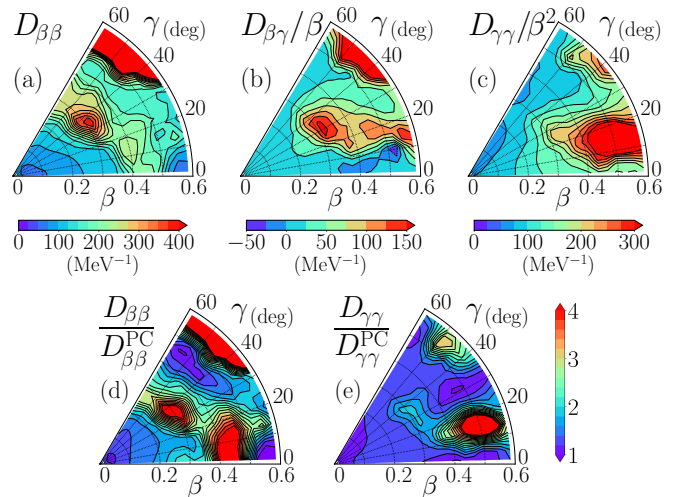


FIG. 2. Vibrational masses of the LQRPA in ^{110}Pd : (a) $D_{\beta\beta}$, (b) $D_{\beta\gamma}/\beta$, and (c) $D_{\gamma\gamma}/\beta^2$. The ratio of the LQRPA to the PC vibrational masses: (d) $D_{\beta\beta}/D_{\beta\beta}^{\text{PC}}$ and (e) $D_{\gamma\gamma}/D_{\gamma\gamma}^{\text{PC}}$.

150 core hours for a contour integration for each deformation point. For the three rotational moments of inertia, it takes about 3 core hours for each deformation point. Computing the LQRPA inertial functions is feasible in currently available computational resources.

Results and discussions. Figure 1(a) shows the calculated potential energy surface (PES) measured from the energy minimum in the β - γ plane in ^{110}Pd . The shallow energy minimum is found at $\beta \approx 0.25$ and $\gamma \approx 0^\circ$. The PES is flat in both the β and γ directions with $V(\beta, \gamma) < 1$ MeV in a wide region of $0.1 < \beta < 0.4$ and $0^\circ < \gamma < 60^\circ$. Figures 1(b) and 1(c) show the pairing gaps for neutrons Δ_n and protons Δ_p , respectively, in ^{110}Pd . The pairing gap in neutrons has local minima at $\beta \approx 0.5, \gamma \approx 15^\circ$ and $\beta \approx 0.6, \gamma \approx 40^\circ$.

Figure 2 shows the vibrational masses $D_{\beta\beta}$ (a), $D_{\beta\gamma}/\beta$ (b), and $D_{\gamma\gamma}/\beta^2$ (c) calculated with the CHFB + LQRPA in the β - γ plane for ^{110}Pd . A remarkable feature is a strong variation of the vibrational masses in the β - γ plane. In particular, the vibrational masses become locally large at around $\beta = 0.5$ and $\gamma = 15^\circ$, $\beta = 0.3$ and $\gamma = 40^\circ$, and $\beta > 0.4$ and $\gamma > 40^\circ$, at which the pairing gaps in neutrons and protons become locally small. A

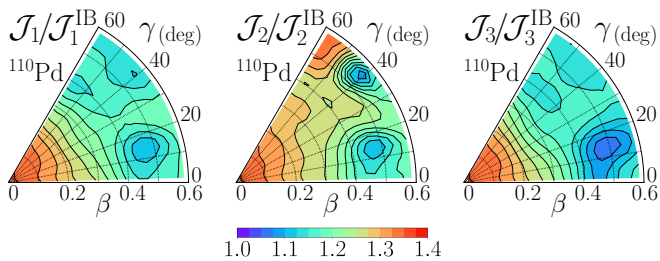


FIG. 3. Ratio of the LQRPA moments of inertia to the Inglis-Beljaev (IB) ones ($\mathcal{J}_k/\mathcal{J}_k^{\text{IB}}$) in the β - γ plane in ^{110}Pd .

correlation between the vibrational mass and pairing gap was also observed in the collective inertia in spontaneous fission [35].

It is of significant importance to compare the vibrational masses obtained by the LQRPA with those obtained by the perturbative cranking (PC) formula [24], denoted as $D_{\beta\beta}^{\text{PC}}$, $D_{\beta\gamma}^{\text{PC}}$, and $D_{\gamma\gamma}^{\text{PC}}$. Those of the PC formula have been extensively employed in the EDF-based 5DCH studies [17, 19, 20]. Figures 2(d) and (e) show the ratio of the LQRPA vibrational mass to the PC one. At a region near the minimum of the PES ($\beta \approx 0.25$ and $\gamma \approx 0^\circ$), the ratio is 1.0–2.0. However, the ratio exceeds 3.0 at the regions at which $D_{\beta\beta}$ and $D_{\gamma\gamma}$ take large values. Furthermore, the ratio shows a strong β - γ dependence and different properties in $D_{\beta\beta}$ and $D_{\gamma\gamma}$. Former EDF-based 5DCH studies have often employed the cranking inertial functions multiplied by a constant enhancement factor to include the dynamical residual effects. However, our findings clearly show that the use of the constant enhancement factor cannot be justified in the description of the vibrational masses. Similar enhancement is observed in the former LQRPA studies with the P + Q model [29, 30, 32] and in those with the axial symmetric restriction [34, 35].

Figure 3 shows the ratios of the LQRPA to the IB cranking moments of inertia $\mathcal{J}_k^{\text{IB}}$ [22, 23] in the β - γ plane for ^{110}Pd . The ratios are in a range of 1.0–1.4 and increase as β decreases; the dynamical residual effects become larger toward the spherical shape. The ratios become small where the pairing gap is small, which is opposite to the case of the vibrational masses. The enhancement is less pronounced than that in the vibrational masses; this indicates the larger dynamical residual effects in the vibrational masses than in the moments of inertia. This is consistent with the LQRPA studies with the P + Q model [29, 30, 32].

Figure 4 shows excitation spectra of the 5DCH for positive-parity I_α^+ states with I being the total angular momentum and α distinguishing the states with the same I and $B(E2)$ values in Weisskopf units in ^{110}Pd . Those of the cranking inertial functions indicate the results obtained with the PC vibrational masses and IB moments of inertia. In the spectra, we show the states with $I \leq 8$ and the excitation energies $E < 2.6$ MeV and the $B(E2)$ values of all the intraband transitions and of the inter-

band ones whose experimental data are available. It is clearly seen that the excitation energies calculated with the LQRPA inertial functions are lower than those calculated with the cranking ones. The enhancement of the LQRPA inertial functions lowers the ground-state rotational energies as well as the excited band-head energies. The low-lying spectra of the LQRPA are in good agreement with the experimental data, showing a clear advantage over those with the cranking inertial functions. However, some discrepancies from the experimental spectra remain particularly at excited bands. For instance, we overestimate the level spacing between 0^+ and 2^+ for the 0_2^+ and the 0_3^+ bands.

The $B(E2)$ values in the ground-state rotational band and $B(E2; 0_2^+ \rightarrow 2_1^+)$ and $B(E2; 2_2^+ \rightarrow 2_1^+)$ agree well with the experimental ones. The $B(E2; 2_3^+ \rightarrow 0_2^+)$ value with the LQRPA underestimates the experimental data, which is related to the overestimation of the level spacing of the 0_2^+ and the 2_3^+ bands. Overall, the dynamical residual effects lead to a better agreement in the property of the low-lying spectra. In contrast to the excitation energies, the $B(E2)$ values calculated with the LQRPA and the cranking inertial functions are similar to each other. It may suggest that the contribution of the dynamical residual effects is more important for the energy properties than for the wave functions, although it is dangerous to generalize the results for other nuclei.

Finally, we discuss the property of shape fluctuations in the low-lying spectra. Figure 5 shows the vibrational wave functions of I_α^+ states as $|\Phi_{\alpha I}(\beta, \gamma)|^2 \equiv \sum_K |\Phi_{\alpha IK}(\beta, \gamma)|^2$ with K being the z component of I in the body-fixed frame. We multiply the wave functions by $\beta^4 \sqrt{W(\beta, \gamma)R(\beta, \gamma)}$ with $W = (D_{\beta\beta}D_{\gamma\gamma} - D_{\beta\gamma}^2)/\beta^2$ and $R = D_1D_2D_3$ from the volume element in the normalization of the vibrational wave functions. The 0_1^+ wave function has a broad peak around $\beta \approx 0.3$, $\gamma \approx 0^\circ$, which is close to the minimum of the PES, and spreads over along both the β and γ directions. This shows that the ground state has a large-amplitude shape fluctuation in the β - γ plane. The 2_1^+ state shows a similar structure but is more localized around $\beta \approx 0.3$, $\gamma \approx 0^\circ$ than the 0_1^+ state is. The 2_2^+ wave function has a broad peak at a triaxial shape $\beta \approx 0.3$ and $\gamma \approx 30^\circ$ and spreads over along the γ direction. The 4_2^+ wave function has a feature similar to the 2_2^+ one, which indicates that the 4_2^+ state is a member of the 2_2^+ band and is localized more in the prolate side. The 0_2^+ and 2_3^+ wave functions show a feature of the β vibration, which has a node along the β direction. However, the component at around $\beta \approx 0.2$ spreads along the γ direction. This reflects a γ -soft character. These collective wave functions clearly show the importance of including the triaxial degree of freedom in the 5DCH for a transitional nucleus ^{110}Pd .

Summary. We have developed a method of calculating the inertial functions of the 5DCH, the vibrational masses and the rotational moments of inertia, by the LQRPA with the Skyrme EDF in the β - γ plane. The method can take into account the time-odd mean fields

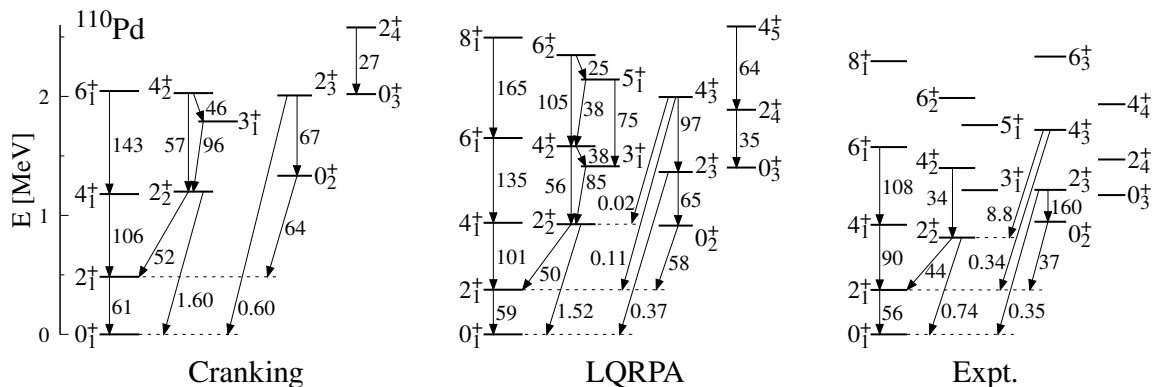


FIG. 4. Low-lying excitation spectra and $B(E2)$ values in Weisskopf units in ^{110}Pd obtained with the cranking inertial functions (left), with the LQRPA ones (middle), compared with the experimental data (right) [63]. See text for details.

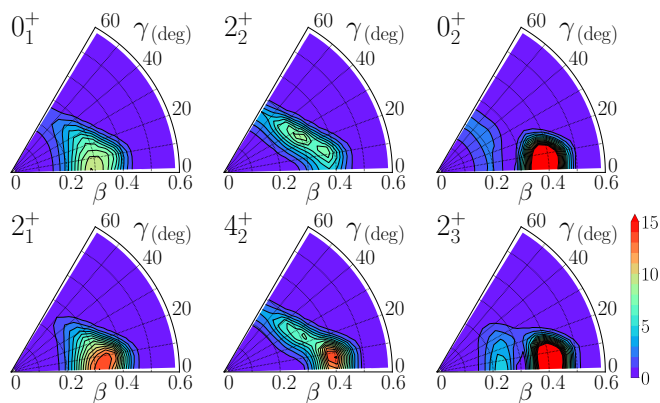


FIG. 5. Vibrational wavefunctions $|\Phi_{\alpha I}(\beta, \gamma)|^2$ of I_{α}^{+} states multiplied by $\beta^4 \sqrt{W(\beta, \gamma)R(\beta, \gamma)}$ in ^{110}Pd .

as the dynamical residual effects in the inertial functions. We constructed the 5DCH with the LQRPA inertial functions and described low-lying states in a transitional nucleus ^{110}Pd . The dynamical residual effects increase both the vibrational masses and rotational moments of inertia, compared with those within the cranking formula. This enhancement strongly depends on both β and γ , which indicates an insufficient treatment of the constant

enhancement factor to the cranking inertial functions employed in former EDF-based 5DCH studies. A good agreement with the experimental data is achieved for low-lying spectra. The vibrational wave functions in the low-lying states show significant shape fluctuations in the β - γ plane.

The present study shows the feasibility of performing computations of the LQRPA for the inertial functions with the present computational resources. However, systematic calculations of the 5DCH method across the nuclear chart will need huge computational costs. Computational costs are expected to be further reduced by using a recent development of the reduced basis method for the FAM [64].

Acknowledgments. The authors thank K. Yaoita for providing his numerical code for solving the collective Schrödinger equation. This work was supported in part by the JSPS KAKENHI (Grant No. JP19KK0343, No. JP20K03964, No. JP22H04569, and No. JP23H01167). Numerical calculations were performed using computational resources of Wisteria/BDEC-01 Odyssey (the University of Tokyo), provided by the Multidisciplinary Cooperative Research Program in the Center for Computational Sciences, University of Tsukuba.

-
- [1] K. Heyde and J. L. Wood, Shape coexistence in atomic nuclei, *Rev. Mod. Phys.* **83**, 1467 (2011).
 - [2] M. Bender, P.-H. Heenen, and P.-G. Reinhard, Self-consistent mean-field models for nuclear structure, *Rev. Mod. Phys.* **75**, 121 (2003).
 - [3] T. Nakatsukasa, K. Matsuyanagi, M. Matsuo, and K. Yabana, Time-dependent density-functional description of nuclear dynamics, *Rev. Mod. Phys.* **88**, 045004 (2016).
 - [4] M. Bender and P.-H. Heenen, Configuration mixing of angular-momentum and particle-number projected triaxial Hartree-Fock-Bogoliubov states using the Skyrme energy density functional, *Phys. Rev. C* **78**, 024309 (2008).
 - [5] J. M. Yao, J. Meng, P. Ring, and D. Vretenar, Configuration mixing of angular-momentum-projected triaxial relativistic mean-field wave functions, *Phys. Rev. C* **81**, 044311 (2010).
 - [6] T. R. Rodríguez and J. L. Egido, Triaxial angular momentum projection and configuration mixing calculations with the Gogny force, *Phys. Rev. C* **81**, 064323 (2010).
 - [7] J. M. Yao, K. Hagino, Z. P. Li, J. Meng, and P. Ring, Microscopic benchmark study of triaxiality in low-lying states of ^{76}Kr , *Phys. Rev. C* **89**, 054306 (2014).
 - [8] M. Kimura, R. Yoshida, and M. Isaka, Excitation and structure change of ^{24}Mg . I: -Triaxial deformed mean

- field in low-lying states–, *Prog. Theor. Phys.* **127**, 287 (2012).
- [9] Y. Suzuki and M. Kimura, Triaxial deformation and the disappearance of the $N = 28$ shell gap, *Phys. Rev. C* **104**, 024327 (2021).
- [10] S. Shinohara, H. Ohta, T. Nakatsukasa, and K. Yabana, Configuration mixing calculation for complete low-lying spectra with a mean-field Hamiltonian, *Phys. Rev. C* **74**, 054315 (2006).
- [11] Y. Fukuoka, S. Shinohara, Y. Funaki, T. Nakatsukasa, and K. Yabana, Deformation and cluster structures in ^{12}C studied with configuration mixing using Skyrme interactions, *Phys. Rev. C* **88**, 014321 (2013).
- [12] M. Matsumoto, Y. Tanimura, and K. Hagino, Extension of the generator coordinate method with basis optimization, *Phys. Rev. C* **108**, L051302 (2023).
- [13] M. Anguiano, J. L. Egido, and L. M. Robledo, Particle number projection with effective forces, *Nucl. Phys. A* **696**, 467 (2001).
- [14] J. Dobaczewski, M. V. Stoitsov, W. Nazarewicz, and P.-G. Reinhard, Particle-number projection and the density functional theory, *Phys. Rev. C* **76**, 054315 (2007).
- [15] A. Bohr and B. R. Mottelson, *Nuclear Structure* (Benjamin, New York, 1975) Vol. II.
- [16] L. Próchniak and S. G. Rohoziński, Quadrupole collective states within the Bohr collective Hamiltonian, *J. Phys. G* **36**, 123101 (2009).
- [17] J. Libert, M. Girod, and J.-P. Delaroche, Microscopic descriptions of superdeformed bands with the Gogny force: Configuration mixing calculations in the $A \sim 190$ mass region, *Phys. Rev. C* **60**, 054301 (1999).
- [18] L. Próchniak, P. Quentin, D. Samsen, and J. Libert, A self-consistent approach to the quadrupole dynamics of medium heavy nuclei, *Nucl. Phys. A* **730**, 59 (2004).
- [19] T. Nikšić, Z. P. Li, D. Vretenar, L. Próchniak, J. Meng, and P. Ring, Beyond the relativistic mean-field approximation. III. Collective Hamiltonian in five dimensions, *Phys. Rev. C* **79**, 034303 (2009).
- [20] J.-P. Delaroche, M. Girod, J. Libert, H. Goutte, S. Hilaire, S. Péru, N. Pillet, and G. F. Bertsch, Structure of even-even nuclei using a mapped collective Hamiltonian and the DIS Gogny interaction, *Phys. Rev. C* **81**, 014303 (2010).
- [21] P. Ring and P. Schuck, *The Nuclear Many-Body Problem* (Springer-Verlag, New York, 1980).
- [22] D. R. Inglis, Nuclear moments of inertia due to nucleon motion in a rotating well, *Phys. Rev.* **103**, 1786 (1956).
- [23] S. T. Beliaev, Concerning the calculation of the nuclear moment of inertia, *Nucl. Phys.* **24**, 322 (1961).
- [24] M. Girod and B. Grammaticos, The zero-point energy correction and its effect on nuclear dynamics, *Nucl. Phys. A* **330**, 40 (1979).
- [25] J. Dobaczewski and J. Skalski, The quadrupole vibrational inertial function in the adiabatic time-dependent Hartree-Fock-Bogolyubov approximation, *Nucl. Phys. A* **369**, 123 (1981).
- [26] K. Wen and T. Nakatsukasa, Microscopic collective inertial masses for nuclear reaction in the presence of nucleonic effective mass, *Phys. Rev. C* **105**, 034603 (2022).
- [27] J.-P. Delaroche, J. Libert, M. Girod, I. Deloncle, and M. Dupuis, Investigations of electric monopole transitions in medium-mass to heavy nuclei: Beyond mean field calculations with the Gogny force, *Phys. Rev. C* **109**, 014320 (2024).
- [28] D. J. Thouless and J. G. Valatin, Time-dependent Hartree-Fock equations and rotational states of nuclei, *Nucl. Phys.* **31**, 211 (1962).
- [29] N. Hinohara, K. Sato, T. Nakatsukasa, M. Matsuo, and K. Matsuyanagi, Microscopic description of large-amplitude shape-mixing dynamics with inertial functions derived in local quasiparticle random-phase approximation, *Phys. Rev. C* **82**, 064313 (2010).
- [30] K. Sato and N. Hinohara, Shape mixing dynamics in the low-lying states of proton-rich Kr isotopes, *Nucl. Phys. A* **849**, 53 (2011).
- [31] N. Hinohara, K. Sato, K. Yoshida, T. Nakatsukasa, M. Matsuo, and K. Matsuyanagi, Shape fluctuations in the ground and excited 0^+ states of $^{30,32,34}\text{Mg}$, *Phys. Rev. C* **84**, 061302(R) (2011).
- [32] N. Hinohara, Z. P. Li, T. Nakatsukasa, T. Nikšić, and D. Vretenar, Effect of time-odd mean fields on inertial parameters of the quadrupole collective Hamiltonian, *Phys. Rev. C* **85**, 024323 (2012).
- [33] K. Sato, N. Hinohara, K. Yoshida, T. Nakatsukasa, M. Matsuo, and K. Matsuyanagi, Shape transition and fluctuations in neutron-rich Cr isotopes around $N = 40$, *Phys. Rev. C* **86**, 024316 (2012).
- [34] K. Yoshida and N. Hinohara, Shape changes and large-amplitude collective dynamics in neutron-rich Cr isotopes, *Phys. Rev. C* **83**, 061302(R) (2011).
- [35] K. Washiyama, N. Hinohara, and T. Nakatsukasa, Finite-amplitude method for collective inertia in spontaneous fission, *Phys. Rev. C* **103**, 014306 (2021).
- [36] T. Nakatsukasa, T. Inakura, and K. Yabana, Finite amplitude method for the solution of the random-phase approximation, *Phys. Rev. C* **76**, 024318 (2007).
- [37] T. Inakura, T. Nakatsukasa, and K. Yabana, Self-consistent calculation of nuclear photoabsorption cross sections: Finite amplitude method with Skyrme functionals in the three-dimensional real space, *Phys. Rev. C* **80**, 044301 (2009).
- [38] P. Avogadro and T. Nakatsukasa, Finite amplitude method for the quasiparticle random-phase approximation, *Phys. Rev. C* **84**, 014314 (2011).
- [39] M. Stoitsov, M. Kortelainen, T. Nakatsukasa, C. Losa, and W. Nazarewicz, Monopole strength function of deformed superfluid nuclei, *Phys. Rev. C* **84**, 041305(R) (2011).
- [40] H. Liang, T. Nakatsukasa, Z. Niu, and J. Meng, Feasibility of the finite-amplitude method in covariant density functional theory, *Phys. Rev. C* **87**, 054310 (2013).
- [41] T. Nikšić, N. Kralj, T. Tutiš, D. Vretenar, and P. Ring, Implementation of the finite amplitude method for the relativistic quasiparticle random-phase approximation, *Phys. Rev. C* **88**, 044327 (2013).
- [42] N. Hinohara, M. Kortelainen, and W. Nazarewicz, Low-energy collective modes of deformed superfluid nuclei within the finite-amplitude method, *Phys. Rev. C* **87**, 064309 (2013).
- [43] M. T. Mustonen, T. Shafer, Z. Zenginerler, and J. Engel, Finite-amplitude method for charge-changing transitions in axially deformed nuclei, *Phys. Rev. C* **90**, 024308 (2014).
- [44] J. C. Pei, M. Kortelainen, Y. N. Zhang, and F. R. Xu, Emergent soft monopole modes in weakly bound deformed nuclei, *Phys. Rev. C* **90**, 051304(R) (2014).
- [45] M. Kortelainen, N. Hinohara, and W. Nazarewicz, Multipole modes in deformed nuclei within the finite amplitude

- method, *Phys. Rev. C* **92**, 051302(R) (2015).
- [46] N. Hinohara, Collective inertia of the Nambu-Goldstone mode from linear response theory, *Phys. Rev. C* **92**, 034321 (2015).
- [47] N. Hinohara and W. Nazarewicz, Pairing Nambu-Goldstone modes within nuclear density functional theory, *Phys. Rev. Lett.* **116**, 152502 (2016).
- [48] K. Wen and T. Nakatsukasa, Self-consistent collective coordinate for reaction path and inertial mass, *Phys. Rev. C* **94**, 054618 (2016).
- [49] K. Washiyama and T. Nakatsukasa, Multipole modes of excitation in triaxially deformed superfluid nuclei, *Phys. Rev. C* **96**, 041304(R) (2017).
- [50] X. Sun and D. Lu, Implementation of a finite-amplitude method in a relativistic meson-exchange model, *Phys. Rev. C* **96**, 024614 (2017).
- [51] N. Hinohara and J. Engel, Global calculation of two-neutrino double- β decay within the finite amplitude method in nuclear density functional theory, *Phys. Rev. C* **105**, 044314 (2022).
- [52] H. Sasaki, T. Kawano, and I. Stetcu, Noniterative finite amplitude methods for $E1$ and $M1$ giant resonances, *Phys. Rev. C* **105**, 044311 (2022).
- [53] K. Petrik and M. Kortelainen, Thouless-Valatin rotational moment of inertia from linear response theory, *Phys. Rev. C* **97**, 034321 (2018).
- [54] K. Washiyama and T. Nakatsukasa, Multipole modes for triaxially deformed superfluid nuclei, *JPS Conf. Proc.* **23**, 013012 (2018).
- [55] K. Matsuyanagi, M. Matsuo, T. Nakatsukasa, K. Yoshida, N. Hinohara, and K. Sato, Microscopic derivation of the Bohr-Mottelson collective Hamiltonian and its application to quadrupole shape dynamics, *Phys. Scr.* **91**, 063014 (2016).
- [56] B. Gall, P. Bonche, J. Dobaczewski, H. Flocard, and P.-H. Heenen, Superdeformed rotational bands in the mercury region. A cranked Skyrme-Hartree-Fock-Bogoliubov study, *Z. Phys. A* **348**, 183 (1994).
- [57] J. Terasaki, P.-H. Heenen, P. Bonche, J. Dobaczewski, and H. Flocard, Superdeformed rotational bands with density dependent pairing interactions, *Nucl. Phys. A* **593**, 1 (1995).
- [58] P. Bonche, H. Flocard, P.-H. Heenen, S. J. Krieger, and M. S. Weiss, Self-consistent study of triaxial deformations: Application to the isotopes of Kr, Sr, Zr and Mo, *Nucl. Phys. A* **443**, 39 (1985).
- [59] P. Bonche, H. Flocard, and P.-H. Heenen, Solution of the Skyrme HF+BCS equation on a 3D mesh, *Comput. Phys. Commun.* **171**, 49 (2005).
- [60] W. Ryssens, V. Hellemans, M. Bender, and P.-H. Heenen, Solution of the Skyrme-HF+BCS equation on a 3D mesh, II: A new version of the ev8 code, *Comput. Phys. Commun.* **187**, 175 (2015).
- [61] V. Hellemans, P.-H. Heenen, and M. Bender, Tensor part of the Skyrme energy density functional. III. Time-odd terms at high spin, *Phys. Rev. C* **85**, 014326 (2012).
- [62] J. Bartel, P. Quentin, M. Brack, C. Guet, and H.-B. Håkansson, Towards a better parametrisation of Skyrme-like effective forces: A critical study of the SkM force, *Nucl. Phys. A* **386**, 79 (1982).
- [63] National Nuclear Data Center, Brookhaven National Laboratory, <https://www.nndc.bnl.gov/nudat3/>.
- [64] N. Hinohara, X. Zhang, and J. Engel, in preparation.